Oncogene (2019) 38:5766–5777
https://doi.org/10.1038/s41388-019-0841-3

ARTICLE

KLF4 as a rheostat of osteolysis and osteogenesis in prostate tumors in the bone

Evelyne Tassone[1] · Vivian Bradaschia-Correa[1,2] · Xiaozhong Xiong[1] · Ana Sastre-Perona[3] · Anne Marie Josephson[1,2] · Alireza Khodadadi-Jamayran[4,5] · Jonathan Melamed[4] · Lei Bu[6] · David J. Kahler[7] · Liliana Ossowski[8] · Philipp Leucht[1,2] · Markus Schober[1,3] · Elaine L. Wilson[1,9]

Received: 9 August 2018 / Revised: 7 May 2019 / Accepted: 8 May 2019 / Published online: 25 June 2019

Abstract

We previously showed that KLF4, a gene highly expressed in murine prostate stem cells, blocks the progression of indolent intraepithelial prostatic lesions into aggressive and rapidly growing tumors. Here, we show that the anti-tumorigenic effect of KLF4 extends to PC3 human prostate cancer cells growing in the bone. We compared KLF4 null cells with cells transduced with a DOX-inducible KLF4 expression system, and find KLF4 function inhibits PC3 growth in monolayer and soft agar cultures. Furthermore, KLF4 null cells proliferate rapidly, forming large, invasive, and osteolytic tumors when injected into mouse femurs, whereas KLF4 re-expression immediately after their intra-femoral inoculation blocks tumor development and preserves a normal bone architecture. KLF4 re-expression in established KLF4 null bone tumors inhibits their osteolytic effects, preventing bone fractures and inducing an osteogenic response with new bone formation. In addition to these profound biological changes, KLF4 also induces a transcriptional shift from an osteolytic program in KLF4 null cells to an osteogenic program. Importantly, bioinformatic analysis shows that genes regulated by KLF4 overlap significantly with those expressed in metastatic prostate cancer patients and in three individual cohorts with bone metastases, strengthening the clinical relevance of the findings in our xenograft model.

Introduction

Prostate cancer is the second most frequently diagnosed tumor in American men [1]. Bone metastases are present in 80% of patients with metastases, and these patients are faced with an incurable disease [2]. A healthy bone is a continuously remodeling organ, characterized by cycles of bone resorption and formation [3]. Disruption of this balance by cancer cells leads to pain, impaired mobility, fractures, spinal cord compression, and hypercalcemia, all causes of morbidity. The metastatic cells divert the bone environment in their favor creating a "vicious cycle" fueled by tumor-secreted

Supplementary information The online version of this article (https://doi.org/10.1038/s41388-019-0841-3) contains supplementary material, which is available to authorized users.

✉ Markus Schober
markus.schober@nyumc.org

✉ Elaine L. Wilson
elaine.wilson@nyumc.org

[1] Department of Cell Biology, NYU School of Medicine, New York, NY 10016, USA

[2] Department of Orthopedic Surgery, NYU School of Medicine, New York, NY 10016, USA

[3] The Ronald O. Perelman Department of Dermatology, NYU School of Medicine, New York, NY 10016, USA

[4] Department of Pathology, NYU School of Medicine, New York, NY 10016, USA

[5] Applied Bioinformatics Laboratories, NYU School of Medicine, New York, NY 10016, USA

[6] Department of Medicine, NYU School of Medicine, New York, NY 10016, USA

[7] High Throughput Biology Laboratory, NYU School of Medicine, New York, NY 10016, USA

[8] Department of Medicine, Mt Sinai School of Medicine, New York, NY 10029, USA

[9] Department of Urology, NYU School of Medicine, New York, NY 10016, USA

factors [4]. Although some of these factors have been identified [5–8], and life-prolonging therapies have been devised [9], many men still succumb to metastatic disease.

We recently identified transcriptional networks that regulate prostate cancer progression [10]. We proposed that overexpression of genes controlling the quiescence of adult prostate stem cells maintains prostate cancer in an indolent state, whereas their loss triggers tumor progression. We showed that decreased expression of one such gene, the cell fate defining transcription factor KLF4 [11], converts tiny prostatic intraepithelial neoplastic lesions into large and aggressive sarcomatoid cancers in a mouse model. Our findings are consistent with previous data showing decreased KLF4 expression in advanced primary prostate cancers [12] and inhibition of prostate tumor growth after its overexpression [13].

KLF4 can have context-dependent oncogenic and tumor suppressive activities [14–16], and it may function differently in primary and metastatic tumors. We therefore aimed to define the function of KLF4 in prostate cancer bone metastases. Because most metastases are detected after hormone ablation therapy, a phase coinciding with the development of androgen resistance, we focused our in vivo work on a hormone-independent cell line, PC3, originally isolated from a bone metastasis [17]. The choice of PC3 was further supported by a recent report [18], which documented a reciprocal upregulation of androgen receptor (AR) and KLF4. Such an interaction might suggest a mechanism for loss of KLF4 in advanced prostate cancer in which AR or its normal function is lost. Here we use PC3 and LNCaP cells to show KLF4 inhibits growth in 2D and 3D cultures. Importantly, we demonstrate KLF4 loss in PC3 cells triggers an invasive and osteolytic phenotype in bone, and KLF4 re-expression restrains tumor growth and stimulates new bone formation. We also uncovered KLF4-regulated transcriptional programs evoking osteolytic and osteogenic responses in the bones of our mouse model and in bone metastases of prostate cancer patients, providing a road map for future mechanistic exploration of the KLF4 effect.

Results

KLF4 inhibits in vitro growth of PC3 and LNCaP cells

To explore the mechanism by which KLF4 exerts its effects on tumor cells, we genomically ablated KLF4 in PC3 cells using CRISPR/Cas9. The homozygote deletion disrupted all KLF4 splice variants and isoforms rendering KLF4 protein undetectable (Fig. 1a, top panel). KLF4 loss increased the anchorage-independent colony-forming ability of PC3 cells in soft agar (Fig. 1a, central and bottom panels). Treatment of null cells transduced with a Tet-ON KLF4 expression construct (KLF4-Tet) with increasing DOX concentrations increased KLF4 protein levels (Fig. 1b, top panel) while reducing, in a dose-dependent manner, their anchorage-dependent proliferation (Fig. 1b, bottom panel). Moreover, induction of KLF4 expression almost completely blocked PC3 growth in soft agar (Fig. 1c). Similar effects of KLF4 were observed in an androgen-sensitive cell line, LNCaP; an increase in KLF4 expression inhibited anchorage-dependent and independent growth (Supplementary Fig. S1).

KLF4 levels in PC3 cells regulate bone remodeling

Prostate cancer metastasizes predominantly to bone and lymph nodes [2]. To study the role of KLF4 in bone tumors,

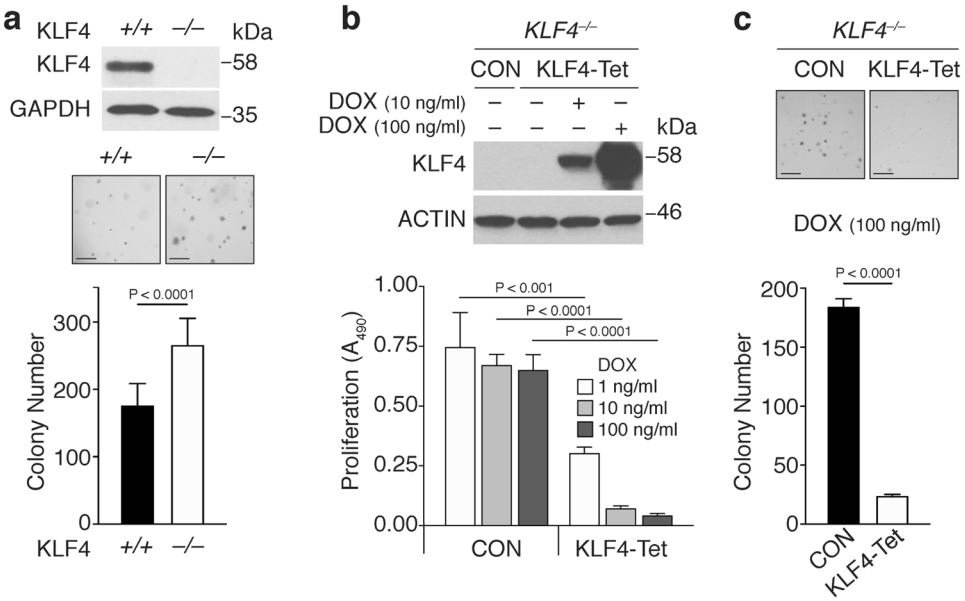

Fig. 1 KLF4 decreases PC3 cell growth. **a** Western blot showing KLF4 absence in null cells (top panel); KLF4 ablation increases 3D growth in soft agar (central and bottom panels). **b** Increasing DOX concentrations in KLF4-Tet cells increases KLF4 protein levels (top panel) and inhibits 2D proliferation (bottom panel) and **c** 3D growth in soft agar. **a**, **c** Representative fields and quantification of colonies grown in soft agar are shown. Experiments were repeated twice. Data represent the mean of technical replicates ± SD. Scale bar = 200 µm

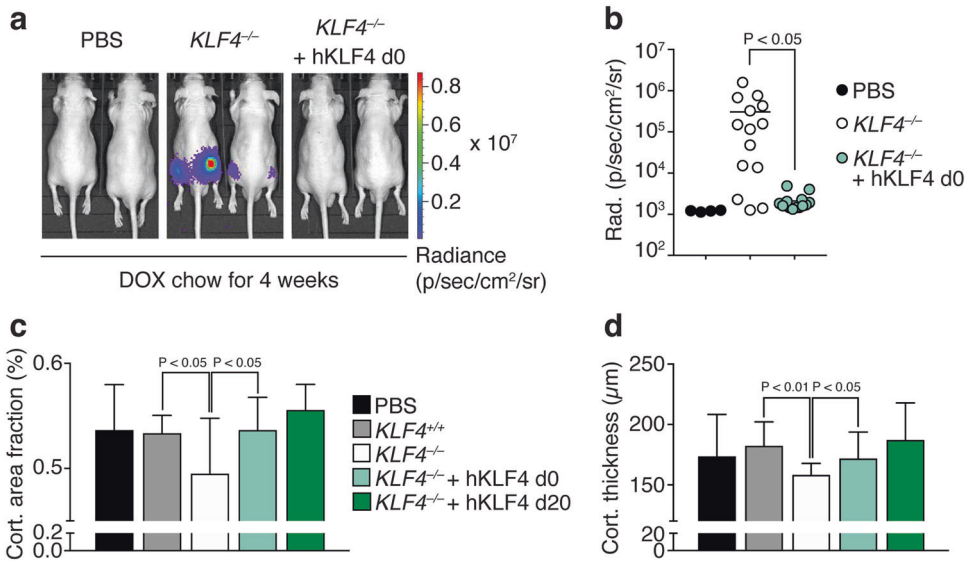

Fig. 2 KLF4 re-expression in PC3 null cells prevents tumor growth in bone. **a** BLI four weeks after intra-femoral injection of null cells ($n = 14$), KLF4-Tet cells ($n = 14$) or PBS ($n = 4$). To induce KLF4, mice were fed DOX-containing chow starting on day 0 (d0). Two representative mice per group are shown. **b** Quantitative analysis of luciferase signal as a measure of tumor growth. Femurs were isolated and analyzed by micro-CT. Two cortical bone parameters were examined: **c** Cortical area fraction and **d** cortical thickness. Data represent the mean of biological replicates (femurs) ± SD. Femurs were inoculated with: PBS ($n = 5$), *KLF4*$^{+/+}$ cells ($n = 11$), *KLF4*$^{-/-}$ cells ($n = 10$), KLF4-Tet cells induced at day 0 ($n = 8$) and day 20 ($n = 7$)

we inoculated PC3 cells, expressing a constitutive GFP-luciferase transgene and different levels of KLF4, intra-femorally. KLF4 was induced in vivo by feeding the mice DOX-containing chow (1 g/kg) (mice cohorts are described in Supplementary Table S1) and tumor growth was monitored periodically by bioluminescence imaging (BLI). At the experimental endpoint, mice were sacrificed and femurs analyzed by micro-CT and histology. Four weeks after cell inoculation and DOX induction, the majority of femurs injected with KLF4 null cells had tumors (11/14), whereas no visible tumors were observed in femurs bearing KLF4-Tet cells (0/14) or in the phosphate-buffered saline (PBS) controls (0/4) (Fig. 2a, b). All mice cohorts were fed DOX-containing chow starting on the day of cell inoculation and continuing for the duration of the experiment (4 weeks).

X-ray radiography revealed fractures, the most extreme signs of bone damage, in two femurs injected with null cells (Supplementary Fig. S2b, c), necessitating the termination of the experiment. No fractures were found in other mice cohorts. Most of the femurs injected with null cells that were analyzed by micro-CT (7/10) showed signs of bone resorption with one or multiple lytic lesions in cortical bone and partial loss of trabecular bone (Fig. 3c, Supplementary Fig. S2h, k, l). These femurs had a decreased cortical area fraction and cortical thickness compared with femurs bearing KLF4-Tet cells fed DOX-containing chow from day 0 (Fig. 2c, d). Histological examination of tumors arising from null cells revealed areas of tumor growth with significant accumulation of osteoclasts (Fig. 3h); in femurs, where tumor cells almost completely filled the bone marrow cavity, cortical and trabecular bone were damaged, and tumor cells invaded the bony collar (Fig. 3h, m). This was not observed in KLF4-expressing tumors (Fig. 3g, l).

In contrast, all femurs bearing KLF4-Tet cells, fed DOX-containing chow and analyzed by micro-CT had normal morphology and no bone resorption (0/8) (Fig. 3d), indicating that early induction of KLF4 prevents tumor growth and protects the bone from destruction. Cortical area fraction and cortical thickness appeared similar to those of femurs injected with wild-type cells (Fig. 2c, d), and their morphology (Fig. 3i, n) was indistinguishable from the PBS controls (Fig. 3a, f, k). Femurs injected with wild-type cells showed osteolytic lesions in only 2/11 femurs (Fig. 3b) and histological analysis confirmed the presence of small, localized tumors (Fig. 3g, l). To ascertain that the observed phenotype is due to KLF4 levels rather than tumor size, we compared a wild-type and a null-generated tumor of similar size; like the two cohorts, the null cell tumor invaded the cortical bone forming lytic lesions, whereas its equal size wild-type cell counterpart formed non-invasive tumors and only partially remodeled the bone (Supplementary Fig. S2e–g vs. h–j).

To mimic the clinical state of advanced bone metastasis, we allowed the bone tumors to grow before we induced KLF4. Twelve femurs were inoculated with KLF4-Tet cells and maintained on a regular diet for 3 weeks at which time (day 20) tumors were detectable in 7/12 femurs (Supplementary Fig. S2d); all mice cohorts were switched to DOX-

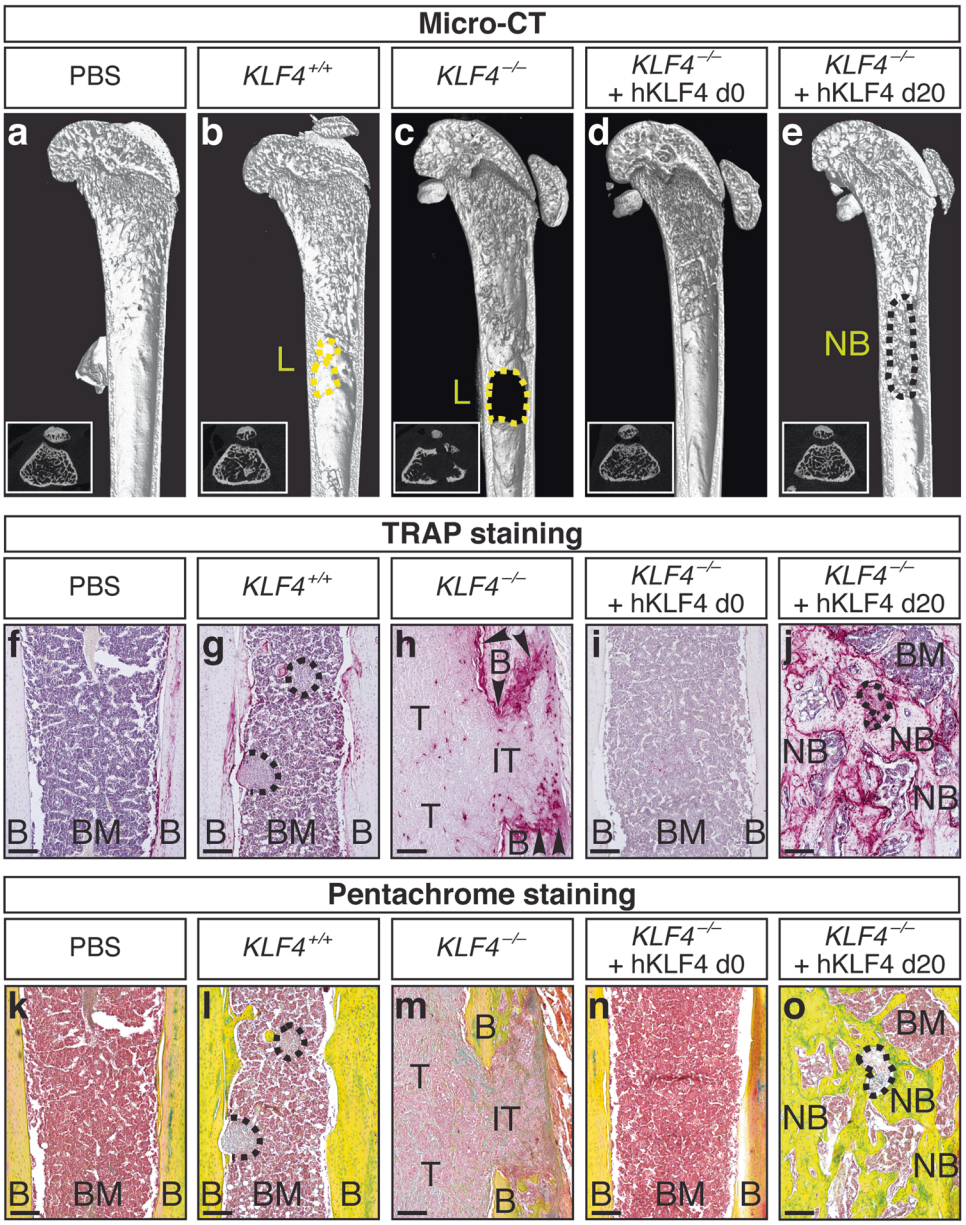

Fig. 3 KLF4 determines osteolytic and osteogenic phenotypes. Micro-CT images of femurs inoculated with **a** PBS, **b** *KLF4*$^{+/+}$ cells, **c** *KLF4*$^{-/-}$ cells, **d** KLF4-Tet cells induced at day 0 and **e** day 20. Small boxed images depict axial sections. L, lytic lesion; NB, new bone; yellow dashed lines, lytic lesions; black dashed line, new bone. **f–j** TRAP and **k–o** pentachrome staining of invasive tumor (IT) and tumor (T), with overt **g**, **h** bone destruction and **o** new bone (NB) formation. B, cortical bone; BM, bone marrow; black dashed lines, tumor areas; black arrows, osteoclasts. Scale bar = 200 µm

containing chow and sacrificed 2 weeks later. Micro-CT analysis indicated a significant osteogenic response in 4/7 femurs in which KLF4 was re-expressed (Fig. 3e, Supplementary Fig. S2m, n). Only small and sparse areas of tumor cells were identified and these areas were surrounded by new bone (Fig. 3j, o), suggesting that KLF4 re-expression reduced tumor size and reversed the damage of advanced bone metastasis.

KLF4-dependent transcriptional programs control osteolytic and osteogenic responses

As most bone metastases go through an initial lytic phase [4], we chose bone metastasis-derived PC3 cells [17], which have an osteolytic phenotype [19] to gain insight into this phase of their growth. We analyzed their transcriptome by RNA-sequencing (RNA-seq) and identified 1542 differentially expressed genes between null and wild-type cells (adjusted P value < 0.05) (Fig. 4a). Because of the profound effects of KLF4 on established tumors, we also examined the transcriptome of null cells after KLF4 re-expression (10 ng/ml DOX) and identified 3959 differentially expressed genes between KLF4 re-expressing cells and null cells (adjusted P value < 0.05) (Fig. 4a). Most of these genes (2599) were upregulated in KLF4 re-expressing cells compared to null cells (Fig. 5b). KLF4 levels in KLF4 re-expressing cells were 20-fold higher than in PC3 wild-type cells, falling within the higher and lower range of KLF4

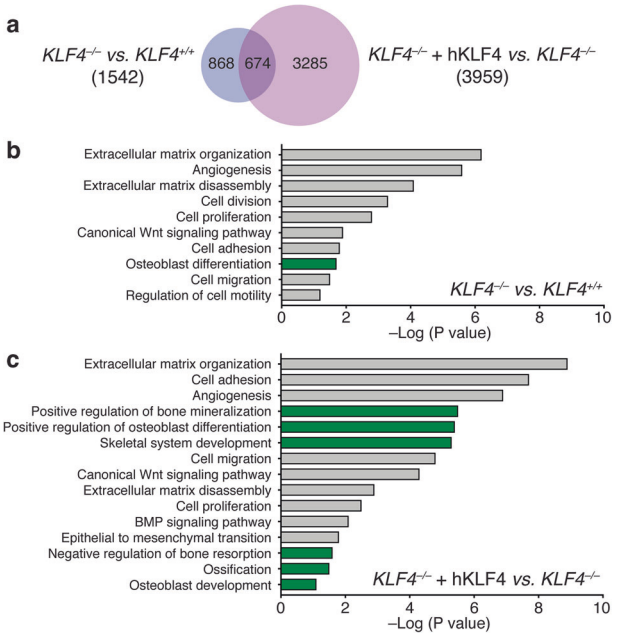

Fig. 4 RNA-seq reveals bone-related pathways. **a** Venn diagram of differentially expressed genes between PC3 null and wild-type cells, and between cells re-expressing KLF4 (by 10 ng/ml DOX) and null cells. **b**, **c** GO analysis indicates KLF4-regulated pathways. Green bars, bone-related pathways. Adjusted *P* value < 0.05

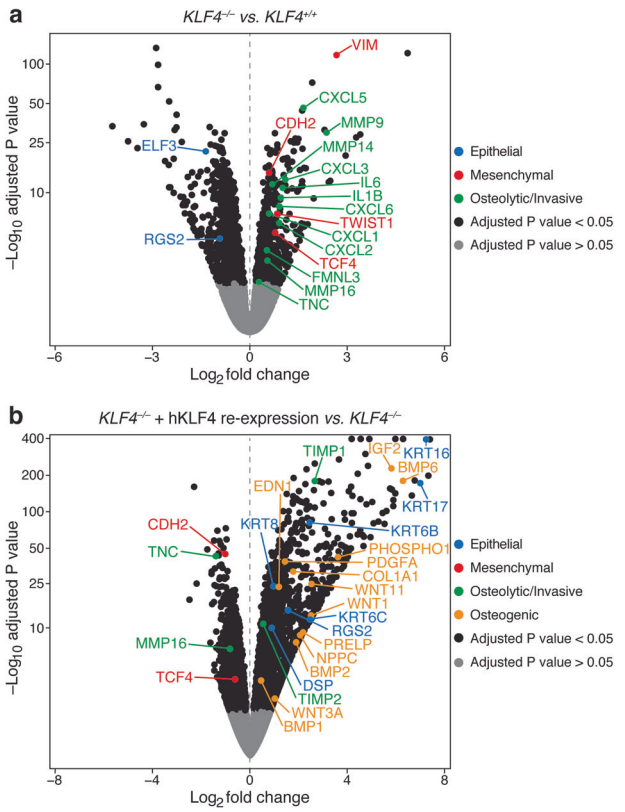

Fig. 5 RNA-seq defines KLF4-dependent transcriptional programs. Volcano plot showing distribution of differentially expressed genes between **a** PC3 null and wild-type cells, and between **b** cells re-expressing KLF4 (by 10 ng/ml DOX) and null cells. Adjusted *P* value < 0.05

expression in primary prostate tumors (Supplementary Fig. S2a) with good and bad prognosis, respectively [10].

In line with the observed phenotypes, Gene Ontology (GO) analysis uncovered pathways related to extracellular matrix (ECM) organization and disassembly, angiogenesis, proliferation, adhesion, and migration (Fig. 4b, c). The expression of several membrane-bound proteins and proteins secreted in the ECM such as matrix metalloproteinases (MMPs) and Tenascin-C (TNC) were identified. MMP9, MMP14, MMP16, TNC, and Formin Like 3 (FMNL3) expression was higher in null compared with wild-type cells (Fig. 5a). Diminished expression of MMP16 and TNC as well as increased expression of MMP16 inhibitors, TIMP1 and TIMP2, were observed in KLF4 re-expressing cells (Fig. 5b).

Genes associated with epithelial–mesenchymal transition (EMT) such as TWIST1, TCF4, CDH2, VIM, and MMP9 were upregulated in null compared to wild-type cells (Fig. 5a), whereas the expression of the epithelial genes, ELF3 and RGS2, was decreased in null compared to wild-type cells (Fig. 5a). We conclude that although null cells retain some aspects of their epithelial identity, the increased expression of mesenchymal markers indicates they have undergone partial EMT. KLF4 re-expressing cells reverted to a more epithelial phenotype, as judged by their expression of cytokeratins (KRT6C, 16 and 17) not normally detected in PC3 cells. We also found increased expression of the epithelial genes RGS2, DSP, KRT6B, and KRT8 and decreased expression of the mesenchymal markers TCF4 and CDH2 in KLF4 re-expressing cells compared with null cells (Fig. 5b). The decreased expression of VIM and MMP9 in KLF4 re-expressing cells, although not statistically significant, confirms the trend towards an epithelial phenotype. These data suggest that KLF4 re-expression in KLF4 deficient cells induces a mesenchymal–epithelial transition.

Remarkably, in support of our in vivo data, we identified numerous bone-related pathways, such as positive regulation of bone mineralization and osteoblast differentiation, skeletal system development, negative regulation of bone resorption, ossification, and osteoblast development (Fig. 4b, c). The expression of several genes known to be important for osteolysis, (IL1B, IL6, MMP9, CXCL1, CXCL2, CXCL3, CXCL5, and CXCL6) [20], was significantly higher in null compared with wild-type cells (Fig. 5a). Increased expression of these KLF4-dependent gene sets may account for the aggressive and osteolytic phenotype of null cells in bone. In addition, KLF4 re-expressing cells had detectable WNT1, WNT3A, WNT11, BMP2, BMP6, NPPC, PRELP, IGF2, and PHOSPHO1 (not expressed in wild-type and null cells), and high expression

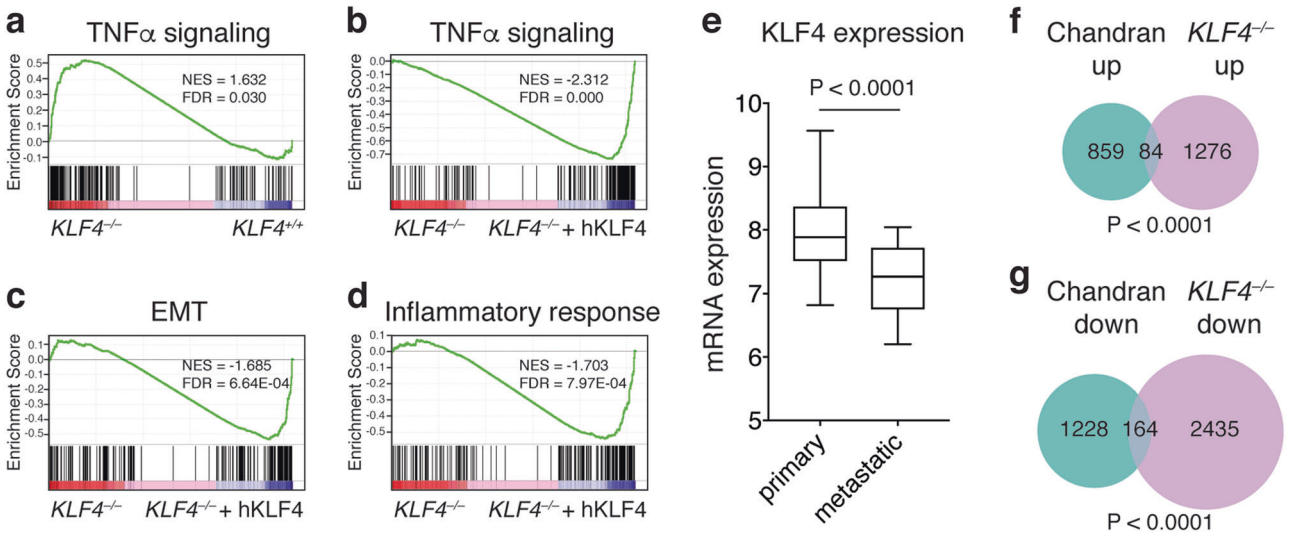

Fig. 6 KLF4 regulates genes and pathways and inversely correlates with the metastatic potential of human prostate cancer. GSEA shows **a** a positive enrichment of the TNFα pathway after KLF4 ablation and **b** a negative enrichment with KLF4 re-expression. GSEA also reveals a positive enrichment of **c** EMT and **d** inflammatory response after KLF4 ablation. **e** Box plot illustrating KLF4 mRNA expression in primary and metastatic prostate cancer specimens [22]. Venn diagrams showing significant overlap between **f** upregulated genes in PC3 null cells and Chandran's [23] data set (84 genes; $P < 0.0001$) and between **g** downregulated genes in null cells and Chandran's data set (164 genes; $P < 0.0001$)

of EDN1, PDGFA, BMP1, and COL1A1 (higher than in null cells) (Fig. 5b).

Gene set enrichment analysis revealed that KLF4 ablation causes a global upregulation of genes associated with TNFα signaling (Fig. 6a). Conversely, KLF4 re-expression represses these genes (Fig. 6b). Thus, KLF4, or the transcriptional program it controls, represses TNFα signaling in prostate cancer cells. Because TNFα induces osteoclastogenesis [21], its repression by KLF4 may explain the osteogenic phenotype of KLF4 re-expressing cells in vivo. Moreover, GSEA confirmed the positive association between reduced KLF4 activity and EMT (Fig. 6c) and it highlighted its involvement in inflammatory responses (Fig. 6d). Taken together, we identified KLF4-dependent transcriptional programs controlling either osteolytic or osteogenic responses in the bone.

KLF4 and its targets have clinical significance in human metastatic prostate cancer

To assess the significance of our xenograft data, we first interrogated the Taylor data set [22] and found an inverse correlation between KLF4 levels and the metastatic potential of human prostate cancer ($P < 0.0001$, Fig. 6e), as previously noted [13]. Next, we intersected the KLF4-regulated gene sets we identified in PC3 cells (Fig. 5) with gene sets which are deregulated in metastases of prostate cancer patients [23]. We identified 84 transcripts common to 1360 genes significantly upregulated in null cells and to 943 genes upregulated in metastatic prostate cancer ($P < 0.0001$; Fig. 6f, Supplementary Table S2). We also uncovered 164 genes common to 2599 genes significantly downregulated in null cells and to 1392 genes downregulated in metastatic prostate cancer patient specimens ($P < 0.0001$; Fig. 6g, Supplementary Table S2).

To establish clinical relevance for the PC3 findings, we examined whether the KLF4-regulated genes linked to osteolysis and osteogenesis are reflected in bone metastases of prostate cancer patients. Interrogation of three independent cohorts [24–26] showed a significant overlap between the 783 upregulated genes in bone metastases from the Kumar and Quigley data sets and the 691 upregulated genes in null cells (45 genes, $P = 1.2E-03$, Fig. 7a, Supplementary Table S2) as well as a significant overlap between the Kumar and Quigley data sets and the 2599 upregulated genes in null cells re-expressing KLF4 (135 genes, $P = 1E-05$, Fig. 7b, Supplementary Table S2). GO analysis on the common gene sets uncovered bone-related pathways, such as osteoblast differentiation and endodermal cell differentiation (Fig. 7c, d). A panel of 10 such genes (MMP9, MMP14, VIM, TWIST1, TNC, FMNL3, BMP1, BMP2, PHOSPHO1, and COL1A1) that were found elevated in the Kumar, Quigley, and Robinson [24–26] cohorts underscores the commonality between KLF4-regulated genes in PC3 cells and bone metastases in prostate cancer patients (Fig. 7e–g), justifying the relevance of our PC3 xenograft model to improve the molecular and physiological understanding of bone metastasis in the future.

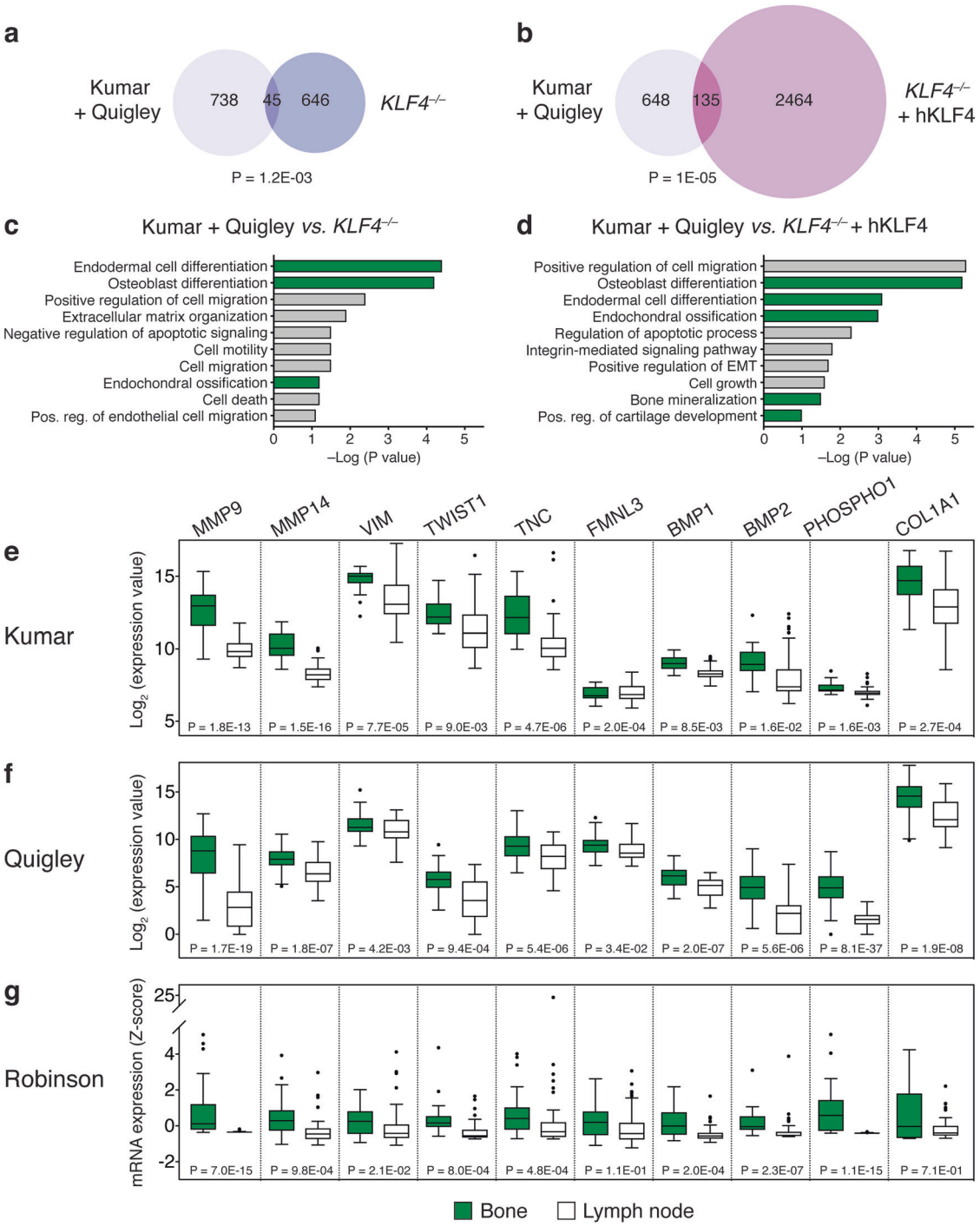

Fig. 7 KLF4-regulated genes are overexpressed in patients with bone metastasis. Venn diagrams showing significant overlap between upregulated genes in Kumar [24] and Quigley [25] bone metastases and upregulated genes in **a** PC3 null cells (45 genes; $P = 1.2E-03$) and **b** cells re-expressing KLF4 (10 ng/ml DOX; 135 genes; $P = 1E-05$). **c**, **d** GO analyses indicate KLF4-regulated pathways. Green bars, bone-related pathways. **e–g** Box plots illustrating gene expression data of candidate genes in bone and lymph node metastases of three independent data sets [24–26]

Discussion

Bone metastases present a significant clinical problem in prostate cancer patients as they cause severe bone damage, extensive pain, and poor survival [2]. Still, how metastatic prostate cancer cells remodel the bone is poorly understood and therapies prolonging patient survival are urgently needed. Here we used PC3 cells, originally isolated from bone metastases of a prostate cancer patient [17], to investigate how KLF4 activity influences their transcriptome, behavior

and pathology. We showed that KLF4 loss is responsible for their aggressive growth and osteolytic phenotype in vivo. Conversely, KLF4 re-expression in null cells, either immediately after bone inoculation or in already established tumors, was able to block tumor growth and protect the bone from resorption.

Our data suggest that KLF4 functions as a tumor suppressor in PC3 and LNCaP cells (Fig. 1, Supplementary Fig. S1), consistent with reports in prostate [12,13, 27] and other cancers [28–31], and we uncover a critical function in bone metastasis that has not previously been reported. Most osteoblastic bone metastases in prostate cancer transit through an initial osteolytic period [4]. However, with few exceptions [32–34], models of mixed bone lesions are still uncommon. That PC3 cells can induce osteolytic lesions in bone has been described [19], but the mechanisms by which this occurs remain elusive. We discovered that KLF4 controls this process by preventing the growth of aggressive bone tumors and by modifying pathways in established tumors that favor osteogenic responses (Fig. 3, Supplementary Fig. S2). This finding has potential therapeutic implications. Indeed, KLF4 has been shown to upregulate the transcription of osteogenic genes in murine smooth muscle cells [35], but inhibition of osteogenesis by KLF4 has also been described [36], suggesting that like the KLF4 context-dependent function in cancer [14], its role in osteogenesis might also require analysis in each specific tissue.

To better understand tumor-related osteolysis and osteogenesis and its dependence on KLF4 levels, we analyzed the transcriptome of PC3 cells. GO analysis uncovered pathways related to bone biology, providing a molecular underpinning to the observed KLF4-dependent in vivo phenotype. Null cells express genes, such as MMPs, compatible with their aggressive, mesenchymal-like and osteolytic phenotype. Although EMT induction by KLF4 downregulation has been described in other cells [10, 12], ours is the first report suggesting a direct link between KLF4-regulated transcription and the KLF4-dependent osteolytic activity of PC3 cells in bone.

Osteoclastogenesis and bone resorption are regulated by RANK, its ligand RANKL, OPG, cytokines, and growth factors [37, 38]. RANK mediates cell migration to the bone and promotes the expression of metastatic genes [20]. Null cells express higher levels of RANK and OPG than wild-type (not shown). Although RANK increase is in line with the strongest osteoclastic activity of null cell-generated tumors, the concomitant OPG increase was unexpected, but possibly counterbalanced by the increased expression of ILs and CXCLs.

In agreement with our results indicating that KLF4 expression induced an osteoblastic phenotype, our RNA-seq analysis identified several genes (WNTs, BMPs, EDN1, PDGFA, NPPC, PRELP, IGF2, and PHOSPHO1) [39–44] that can explain the osteoblastic response. Wnt signaling promotes osteoblast differentiation, contributing to the formation of osteoblastic lesions [39], and this pathway is activated in metastatic castration-resistant prostate cancer [26]. The fact that KLF4 reduces tumor burden and increases the level of osteoblast-promoting genes and new bone formation suggests a new approach to alleviation of bone metastasis and morbidity. However, before this approach can be tested clinically, further study of the quality of the newly deposited bone has to be undertaken to assure it is physiologically normal.

Another important and novel role for KLF4 we identified is the repression of TNFα signaling (Fig. 6). Although the function of TNFα in bone homeostasis is still debated [45], it is currently believed that TNFα induces osteoclastogenesis [21] and inhibits osteoblastogenesis [46]. Thus, the KLF4-dependent repression of TNFα is likely to account for the osteogenic behavior of KLF4 re-expressing cells in vivo. The significant overlap between KLF4-regulated genes and metastatic genes (Fig. 6), together with the finding that expression of a number of these genes (MMP9, MMP14, VIM, TWIST1, TNC, FMNL3, BMP1, BMP2, PHOSPHO1, and COL1A1) specifically increases in bone metastases of patients in three independent cohorts [23–26] (Fig. 7), provides clinical significance to our xenograft model and data.

Using PC3 cells as a model of hormone-independent prostate cancer, we identified novel and important pathways, such as Wnt and TNFα, through which KLF4 switches tumor cell programs in favor of osteogenesis. We also uncovered a clinically-relevant network of KLF4-regulated genes that might serve as a basis for the development of new therapeutic targets for advanced prostate cancer. These findings provide a significant platform for future testing of specific mechanisms that govern the profound KLF4-regulated changes.

Material and methods

Cell culture

PC3 and LNCaP cells (ATCC, Manassas, VA, USA) were cultured in Roswell Park Memorial Institute (RPMI) with 10% fetal bovine serum, 100 µg/ml streptomycin, 100 U/ml penicillin, and 2 mmol/l glutamine (Corning Cellgro, VA, USA), and maintained in a humidified atmosphere of 5% CO_2 at 37 °C. Cells were authenticated by short tandem repeat profiling and tested for mycoplasma. Two guide RNAs specific to human KLF4 (5′-CCCCGAATAACGT GAGTATCGCT-3′ and 5′-CCCACACTTGTGATTACG CGGGC-3′) were cloned into the pSpCas9(BB)-2A-GFP

(PX458) vector [47] and transiently transfected into PC3 cells using Fugene6 (Promega, WI, USA). Green fluorescent protein (GFP)-positive cells were sorted and subcloned. KLF4 wild-type and null clones were sequenced and verified by western blot. GFP loss indicated that neither Cas9 nor the sgRNAs were integrated in their genome.

Lentiviral constructs and infection

To re-express KLF4, we used a DOX-inducible Tet-ON lentiviral system. We modified the vector FUW-tetO-hKLF4 [48] by inserting the sequence of BFP-T2A-hKLF4 or BFP-T2A. To generate GFP-luciferase cells, we used the lentiviral construct BLIV513PA-1 (System Biosciences, CA, USA). Lentiviruses were produced in HEK293T cells as described [10]. BFP-T2A-hKLF4 or BFP-T2A expression was induced by DOX (Sigma-Aldrich, MO, USA).

Western blot

Western blot was performed as described [10]. Anti-KLF4 primary antibody (sc-20691; dilution 1:1000; Santa Cruz Biotechnology, Dallas, TX, USA) was used with GAPDH (5174; dilution 1:10000; Cell Signaling Technologies, Danvers, MA, USA) or ACTIN (A5441; dilution 1:10000; Sigma-Aldrich) as a loading control. Membranes were incubated with rabbit or mouse horseradish peroxidase-conjugated secondary antibodies (HAF008 and HAF007; dilutions range 1:5000–1:20000; R&D Systems, Minneapolis, MN, USA).

Cell proliferation

PC3 null and LNCaP cells (2×10^3 cells/well) were seeded in 96-well plates. Cells expressing the BFP-T2A-hKLF4 construct (KLF4-Tet) as well as the control vector BFP-T2A were incubated with or without DOX up to 4 (LNCaP) or 5 (PC3) days. DOX (1, 10, or 100 ng/ml) was added on day 0 and replaced at 48-hour intervals. Cell proliferation was evaluated using the MTS kit (PC3) or the CellTiter kit (LNCaP) (Promega). Experiments were repeated twice. Data are expressed as the mean of at least three technical replicates ± SD. No data were excluded.

Growth in soft agar

PC3 (2.5×10^3 cells/well) and LNCaP (4×10^3 cells/well) cells were mixed with 0.6% agarose in a 1:1 ratio and seeded into 24-well plates pre-coated with 0.5% agarose [49]. KLF4-Tet and control cells were incubated with or without DOX up to 13 (PC3) or 23 (LNCaP) days. DOX (10 or 100 ng/ml for LNCaP or PC3, respectively) was added on day 0 and replaced at 48-hour intervals. Colonies were imaged using the Thermo Cellomics ArrayScan VTI (Thermo Fisher Scientific) and images processed with JMP Pro v13. Colonies with a diameter greater than 50 µm were scored. Experiments were repeated twice. Data are expressed as the mean of at least three technical replicates ± SD. No data were excluded.

Animal studies

Wild-type, null and KLF4-Tet cells (10^5 cells) as well as PBS were injected into both femurs of 6-weeks old male athymic nude mice (strain code: 490; Charles River, MA, USA; $n = 6$, 12, 13, 3 mice, respectively). No statistical method was used to predetermine sample size, which was based on similar studies and was sufficient to determine significance. Mice were randomly assigned to experimental groups; no particular method of randomization was used; investigators were not blinded. Mice were fed normal or DOX chow (1 g/kg, Bio Serv, NJ, USA) ad libitum starting at day 0 or 20. Bone lesions and tumor growth were monitored by X-ray and BLI with IVIS Lumina-III-XR (PerkinElmer, MA, USA). Images were analyzed by Living Image Software and plotted as average radiance (p/sec/cm^2/sr). At the experimental endpoint, eight mice (four with null cells, two with KLF4-Tet cells + hKLF4 d0 and two with KLF4-Tet cells + hKLF4 d20) were used for other purposes. The remaining femurs were fixed in 4% PFA overnight at 4 °C and scanned using a micro-CT scanner (SkyScan 1172, Bruker, Billerica, MA, USA). Images were reconstructed and analyzed in Dataviewer and CTan. We quantified cortical area fraction (Bone Area/Total Area) and cortical thickness [50], excluding femurs with aberrant injections or bone fractures (Supplementary Table S1). All animal studies were performed in accordance with the guidelines and approval of the Institutional Animal Care and Use Committee at NYU School of Medicine.

Histological analysis

Fixed femurs were decalcified in 19% ethylenediaminetetraacetic acid (pH 7.4) for 21 days, dehydrated in a graded ethanol series, embedded in paraffin and cut into 10-µm-thick sections. Pentachrome staining was used to detect bone [51]. Tartrate-resistant acid phosphatase staining was performed with the Leukocyte Acid Phosphatase kit (Sigma-Aldrich). Pathological examination of histological sections was carried out by two independent investigators who were blind to experimental conditions.

RNA-sequencing and data processing

Differential gene expression between null and wild-type cells, and between cells re-expressing KLF4 and null cells

was measured by RNA-seq. Uninfected null and wild-type cells as well as KLF4-Tet cells (null cells expressing the BFP-T2A-hKLF4 construct) and their control cells (null cells expressing the BFP-T2A construct) incubated with DOX (10 ng/ml) were harvested after 48 hours. Total RNA was extracted using the RNeasy kit (Qiagen, CA, USA). RNA samples were submitted in duplicate. RNA-seq libraries were prepared with the TruSeq sample preparation kit (Illumina, CA, USA). Sequencing reads were mapped to the human genome (GRCh37/hg19) using the STAR aligner (v2.5.0c) [52]. Alignments were guided by a Gene Transfer Format file (Ensembl GTF version GRCh37.70). The mean read insert sizes and their standard deviations were calculated using Picard tools (v.1.126). The read count tables were generated using HTSeq (v0.6.0) [53], normalized based on their library size factors using DESeq (v3.7) [54], and differential expression analysis was performed. The Read Per Million normalized BigWig files were generated using BEDTools (v2.17.0) [55] and bedGraphToBigWig tool (v4). Statistical analyses were performed with R (v3.1.1), GO analysis with David Bioinformatics Resources 6.8 [56, 57] and GSEA with the hallmarks (h.all.v6.1.symbols.gmt) gene sets of the Molecular Signature Database (MSigDB) v6.1 [58, 59]. KLF4 RNA expression levels in wild-type and KLF4 re-expressing cells were ascertained by RNA-seq and compared with a primary prostate adenocarcinoma cohort (TCGA, Provisional) of 499 patients on cBioPortal [60, 61]. Initial raw data analysis was blinded.

Analysis of KLF4 and its target genes in human prostate cancer cohorts

To test whether the KLF4-dependent genes that we identified are differentially expressed between primary and metastatic prostate cancers [23], we re-analyzed the Chandran data set with GEO2R. Genes significantly upregulated and downregulated in KLF4 re-expressing cells compared with null cells were intersected with genes upregulated and downregulated in the data set [23]. Statistical significance was calculated with Fisher's exact test. To determine the clinical relevance of KLF4 and its regulated genes in metastatic patients, we analyzed differences in gene expression between primary ($n = 109$) and metastatic ($n = 19$) prostate tumors [22], and between bone and lymph node metastases from three data sets: Kumar ($n = 20$ vs. $n = 69$) [24], Quigley ($n = 43$ vs. $n = 35$) [25] and Robinson ($n = 29$ vs. $n = 50$) [26]. Genes significantly upregulated in bone compared to lymph node metastases from the Kumar and Quigley cohorts were intersected with genes upregulated in KLF4 null cells and KLF4 re-expressing cells. Monte Carlo simulations with 100,000 iterations indicate that the overlap is statistically significant. David Bioinformatics Resources revealed significantly enriched GO categories. Gene expression levels are illustrated as Box plots (Tukey), and statistical significance was determined by Wilcoxon non-parametric *t* test (Taylor), GEO2R (Kumar), DEseq2 (Quigley) and Mann–Whitney non-parametric *t* tests (Robinson).

Data deposition

Sequencing data are available under the accession number GSE117965.

Statistical analysis

Statistical differences were measured using the 2-tailed unpaired Student's *t* test, unless otherwise specified. All tests were done in GraphPad Prism7 or R. A P value of < 0.05 is considered statistically significant.

Acknowledgements We thank Dr. E. Hernando-Monge (NYU School of Medicine) for the GFP-luciferase plasmid (BLIV513PA-1) and Drs. S. Logan and M. Garabedian (NYU School of Medicine) for helpful discussions. This study was supported by the NIH (R01CA132641 to E.L.W., R01AG056169 and K08AR069099 to P.L., R01CA181111 to M.S., T32CA009161 and T32AR064184 to A.S-P.), the American Cancer Society (RSG-16-033-01-DDC to M.S.), the Department of Urology and the Kimmel Center for Stem Cell Biology. Core funding (Applied Bioinformatics Laboratories, Genome Technology Center, High Throughput Biology Laboratory, Experimental Pathology Research Laboratory, Micro-CT) is partially supported by the Perlmutter Cancer Center (P30CA016087), NYSTEM (contract C026719), and NIH (S10 OD010751).

Author contributions E.T., P.L., M.S., and E.L.W. conceived and designed the study. E.T., V.B-C., X.X., and A.M.J. performed the experiments and analyzed the data. M.S., A.S-P., and A.K-J. performed the bioinformatics analysis. J.M. and P.L. interpreted histological data. L.B. provided the BFP sequence of the KLF4-expressing vector and helped with the cloning strategy. D.J.K. acquired the images of soft agar cultures and analyzed the data. E.T., L.O., M.S., and E.L.W. wrote the manuscript. All authors revised and approved the manuscript.

Compliance with ethical standards

Conflict of interest The authors declare that they have no conflict of interest.

Publisher's note: Springer Nature remains neutral with regard to jurisdictional claims in published maps and institutional affiliations.

References

1. Siegel RL, Miller KD, Jemal A. Cancer statistics, 2018. CA Cancer J Clin 2018;68:7–30.
2. Vela I, Gregory L, Gardiner EM, Clements JA, Nicol DL. Bone and prostate cancer cell interactions in metastatic prostate cancer. BJU Int 2007;99:735–42.
3. Crockett JC, Rogers MJ, Coxon FP, Hocking LJ, Helfrich MH. Bone remodelling at a glance. J Cell Sci 2011;124:991–8.

4. Park SH, Keller ET, Shiozawa Y. Bone marrow microenvironment as a regulator and therapeutic target for prostate cancer bone metastasis. Calcif Tissue Int 2018;102:152–62.
5. Sims NA. Cell-specific paracrine actions of IL-6 family cytokines from bone, marrow and muscle that control bone formation and resorption. Int J Biochem Cell Biol 2016;79:14–23.
6. Gooding S, Edwards CM. New approaches to targeting the bone marrow microenvironment in multiple myeloma. Curr Opin Pharmacol 2016;28:43–9.
7. Nandana S, Tripathi M, Duan P, Chu C-Y, Mishra R, Liu C, et al. Bone metastasis of prostate cancer can be therapeutically targeted at the TBX2-WNT signaling axis. Cancer Res 2017;77:1331–44.
8. Wu JB, Yin L, Shi C, Li Q, Duan P, Huang J-M, et al. MAOA-dependent activation of Shh-IL6-RANKL signaling network promotes prostate cancer metastasis by engaging tumor-stromal cell interactions. Cancer Cell 2017;31:368–82.
9. Body J-J, Casimiro S, Costa L. Targeting bone metastases in prostate cancer: improving clinical outcome. Nat Rev Urol 2015;12:340–56.
10. Xiong X, Schober M, Tassone E, Khodadadi-Jamayran A, Sastre Perona A, Zhou H, et al. KLF4, A gene regulating prostate stem cell homeostasis, is a barrier to malignant progression and predictor of good prognosis in prostate cancer. Cell Rep 2018;25:3006–20.
11. Takahashi K, Yamanaka S. Induction of pluripotent stem cells from mouse embryonic and adult fibroblast cultures by defined factors. Cell 2006;126:663–76.
12. Liu YN, Abou-Kheir W, Yin JJ, Fang L, Hynes P, Casey O, et al. Critical and reciprocal regulation of KLF4 and SLUG in transforming growth factor β-initiated prostate cancer epithelial-mesenchymal transition. Mol Cell Biol 2012;32:941–53.
13. Wang J, Place RF, Huang V, Wang X, Noonan EJ, Magyar CE, et al. Prognostic value and function of KLF4 in prostate cancer: RNAa and vector-mediated overexpression identify KLF4 as an inhibitor of tumor cell growth and migration. Cancer Res 2010;70:10182–91.
14. Rowland BD, Peeper DS. KLF4, p21 and context-dependent opposing forces in cancer. Nat Rev Cancer 2005;6:11–23.
15. Tetreault M-P, Yang Y, Katz JP. Krüppel-like factors in cancer. Nat Rev Cancer 2013;13:701–13.
16. Ghaleb AM, Yang VW. Krüppel-like factor 4 (KLF4): what we currently know. Gene 2017;611:27–37.
17. Kaighn ME, Narayan KS, Ohnuki Y, Lechner JF, Jones LW. Establishment and characterization of a human prostatic carcinoma cell line (PC-3). Invest Urol 1979;17:16–23.
18. Siu M-K, Suau F, Chen W-Y, Tsai Y-C, Tsai H-Y, Yeh H-L, et al. KLF4 functions as an activator of the androgen receptor through reciprocal feedback. Oncogenesis 2016;5:e282.
19. Sanchez-Sweatman OH, Orr FW, Singh G. Human metastatic prostate PC3 cell lines degrade bone using matrix metalloproteinases. Invasion Metastasis 1998;18:297–305.
20. Armstrong AP, Miller RE, Jones JC, Zhang J, Keller ET, Dougall WC. RANKL acts directly on RANK-expressing prostate tumor cells and mediates migration and expression of tumor metastasis genes. Prostate 2007;68:92–104.
21. Kudo O, Fujikawa Y, Itonaga I, Sabokbar A, Torisu T, Athanasou NA. Proinflammatory cytokine (TNFα/IL-1α) induction of human osteoclast formation. J Pathol 2002;198:220–7.
22. Taylor BS, Schultz N, Hieronymus H, Gopalan A, Xiao Y, Carver BS, et al. Integrative genomic profiling of human prostate cancer. Cancer Cell 2010;18:11–22.
23. Chandran UR, Ma C, Dhir R, Bisceglia M, Lyons-Weiler M, Liang W, et al. Gene expression profiles of prostate cancer reveal involvement of multiple molecular pathways in the metastatic process. BMC Cancer 2007;7:64.
24. Kumar A, Coleman I, Morrissey C, Zhang X, True LD, Gulati R, et al. Substantial interindividual and limited intraindividual genomic diversity among tumors from men with metastatic prostate cancer. Nat Med 2016;22:369–78.
25. Quigley DA, Dang HX, Zhao SG, Lloyd P, Aggarwal R, Alumkal JJ, et al. Genomic hallmarks and structural variation in metastatic prostate. Cancer Cell 2018;174:758–769.e9.
26. Robinson D, Van Allen EM, Wu Y-M, Schultz N, Lonigro RJ, Mosquera J-M, et al. Integrative clinical genomics of advanced prostate cancer. Cell 2015;161:1215–28. May
27. Chen X, Whitney EM, Gao SY, Yang VW. Transcriptional profiling of Krüppel-like factor 4 reveals a function in cell cycle regulation and epithelial differentiation. J Mol Biol 2003;326:665–77.
28. Rowland BD, Bernards R, Peeper DS. The KLF4 tumour suppressor is a transcriptional repressor of p53 that acts as a context-dependent oncogene. Nat Cell Biol 2005;7:1074–82.
29. Zhao W, Hisamuddin IM, Nandan MO, Babbin BA, Lamb NE, Yang VW. Identification of Krüppel-like factor 4 as a potential tumor suppressor gene in colorectal cancer. Oncogene 2004;23:395–402.
30. Wei D, Gong W, Kanai M, Schlunk C, Wang L, Yao JC, et al. Drastic down-regulation of Krüppel-like factor 4 expression is critical in human gastric cancer development and progression. Cancer Res 2005;65:2746–54.
31. Sastre-Perona A, Hoang-Phou S, Leitner MC, Okuniewska M, Meehan S, Schober M. De novo PITX1 expression controls bistable transcriptional circuits to govern self-renewal and differentiation in squamous cell carcinoma. Cell Stem Cell 2019;24:390–404.
32. Fradet A, Sorel H, Depalle B, Serre CM, Farlay D, Turtoi A, et al. A new murine model of osteoblastic/osteolytic lesions from human androgen-resistant prostate cancer. PLoS ONE 2013;8:e75092.
33. Li ZG, Mathew P, Yang J, Starbuck MW, Zurita AJ, Liu J, et al. Androgen receptor-negative human prostate cancer cells induce osteogenesis in mice through FGF9-mediated mechanisms. J Clin Invest 2008;118:2697–710.
34. LeRoy BE, Thudi NK, Nadella MVP, Toribio RE, Tannehill-Gregg SH, van Bokhoven A, et al. New bone formation and osteolysis by a metastatic, highly invasive canine prostate carcinoma xenograft. Prostate 2006;66:1213–22.
35. Yoshida T, Yamashita M, Hayashi M. Kruppel-like factor 4 contributes to high phosphate-induced phenotypic switching of vascular smooth muscle cells into osteogenic cells. J Biol Chem 2012;287:25706–14.
36. Barba M, Pirozzi F, Saulnier N, Vitali T, Natale MT, Logroscino G, et al. Lim mineralization protein 3 induces the osteogenic differentiation of human amniotic fluid stromal cells through kruppel-like factor-4 downregulation and further bone-specific gene expression. J Biomed Biotechnol 2012;2012:1–11.
37. Boyle WJ, Simonet WS, Lacey DL. Osteoclast differentiation and activation. Nature 2003;423:337–42.
38. Sottnik JL, Keller ET. Understanding and targeting osteoclastic activity in prostate cancer bone metastases. Curr Mol Med. 2013;13:626–39.
39. Gaur T, Lengner CJ, Hovhannisyan H, Bhat RA, Bodine PVN, Komm BS, et al. Canonical WNT signaling promotes osteogenesis by directly stimulating Runx2 gene expression. J Biol Chem 2005;280:33132–40.
40. Hopkins DR, Keles S, Greenspan DS. The bone morphogenetic protein 1/Tolloid-like metalloproteinases. Matrix Biol 2007;26:508–23.
41. Tsuji T, Kondo E, Yasoda A, Inamoto M, Kiyosu C, Nakao K, et al. Hypomorphic mutation in mouse Nppc gene causes retarded bone growth due to impaired endochondral ossification. Biochem Biophys Res Commun 2008;376:186–90.
42. Rucci N, Rufo A, Alamanou M, Capulli M, Del Fattore A, Åhrman E, et al. The glycosaminoglycan-binding domain of PRELP

acts as a cell type-specific NF-κB inhibitor that impairs osteoclastogenesis. J Cell Biol 2009;187:669–83.
43. Uchimura T, Hollander JM, Nakamura DS, Liu Z, Rosen CJ, Georgakoudi I, et al. An essential role for IGF2 in cartilage development and glucose metabolism during postnatal long bone growth. Development 2017;144:3533–46.
44. Morcos MW, Al-Jallad H, Li J, Farquharson C, Millán JL, Hamdy RC, et al. PHOSPHO1 is essential for normal bone fracture healing. Bone Jt Res 2018;7:397–405.
45. Osta B, Benedetti G, Miossec P. Classical and paradoxical effects of TNF-α on bone homeostasis. Front Immunol 2014;5:48.
46. Lee H-L, Yi T, Woo KM, Ryoo H-M, Kim G-S, Baek J-H. Msx2 mediates the inhibitory action of TNF-α on osteoblast differentiation. Exp Mol Med 2010;42:437–9.
47. Ran FA, Hsu PD, Wright J, Agarwala V, Scott DA, Zhang F. Genome engineering using the CRISPR-Cas9 system. Nat Protoc 2013;8:2281–308.
48. Hockemeyer D, Soldner F, Cook EG, Gao Q, Mitalipova M, Jaenisch R. A drug-inducible system for direct reprogramming of human somatic cells to pluripotency. Cell Stem Cell 2008;3:346–53.
49. Borowicz S, Van Scoyk M, Avasarala S, Karuppusamy Rathinam MK, Tauler J, Bikkavilli RK, et al. The soft agar colony formation assay. J Vis Exp 2014;92:1–6.
50. Bouxsein ML, Boyd SK, Christiansen BA, Guldberg RE, Jepsen KJ, Müller R. Guidelines for assessment of bone microstructure in rodents using micro-computed tomography. J Bone Min Res 2010;25:1468–86.
51. Leucht P, Kim J-B, Wazen R, Currey JA, Nanci A, Brunski JB, et al. Effect of mechanical stimuli on skeletal regeneration around implants. Bone 2007;40:919–30.
52. Dobin A, Davis CA, Schlesinger F, Drenkow J, Zaleski C, Jha S, et al. STAR: ultrafast universal RNA-seq aligner. Bioinformatics 2012;29:15–21.
53. Anders S, Pyl PT, Huber W. HTSeq-a Python framework to work with high-throughput sequencing data. Bioinformatics 2015;31:166–9.
54. Anders S, Huber W. Differential expression analysis for sequence count data. Genome Biol 2010;11:R106.
55. Quinlan AR, Hall IM. BEDTools: a flexible suite of utilities for comparing genomic features. Bioinformatics 2010;26:841–2.
56. Huang DW, Sherman BT, Lempicki RA. Systematic and integrative analysis of large gene lists using DAVID bioinformatics resources. Nat Protoc 2009;4:44–57.
57. Huang DW, Sherman BT, Lempicki RA. Bioinformatics enrichment tools: paths toward the comprehensive functional analysis of large gene lists. Nucleic Acids Res 2008;37:1–13.
58. Subramanian A, Tamayo P, Mootha VK, Mukherjee S, Ebert BL, Gillette MA, et al. Gene set enrichment analysis: a knowledge-based approach for interpreting genome-wide expression profiles. Proc Natl Acad Sci USA 2005;102:15545–50.
59. Mootha VK, Lindgren CM, Eriksson K-F, Subramanian A, Sihag S, Lehar J, et al. PGC-1alpha-responsive genes involved in oxidative phosphorylation are coordinately downregulated in human diabetes. Nat Genet 2003;34:267–73.
60. Gao J, Aksoy BA, Dogrusoz U, Dresdner G, Gross B, Sumer SO, et al. Integrative analysis of complex cancer genomics and clinical profiles using the cBioPortal. Sci Signal 2013;6:pl1.
61. Cerami E, Gao J, Dogrusoz U, Gross BE, Sumer SO, Aksoy BA, et al. The cBio cancer genomics portal: an open platform for exploring multidimensional cancer genomics data. Cancer Discov 2012;2:401–4.